Journal of Power Sources 269 (2014) 194–202

Contents lists available at ScienceDirect

Journal of Power Sources

journal homepage: www.elsevier.com/locate/jpowsour

Ionic conductor cerous phosphate and carbon hybrid coating $LiFePO_4$ with improved electrochemical properties for lithium ion batteries

Zhipeng Ma [a, b], Guangjie Shao [a, b, *], Xiujuan Qin [a, b, *], Yuqian Fan [a, b], Guiling Wang [a, b], Jianjun Song [a, b], Tingting Liu [a, b]

[a] State Key Laboratory of Metastable Materials Science and Technology, Yanshan University, Qinhuangdao 066004, China
[b] Hebei Key Laboratory of Applied Chemistry, College of Environmental and Chemical Engineering, Yanshan University, Qinhuangdao 066004, China

HIGHLIGHTS

- Novel cerous phosphate and carbon hybrid coating $LiFePO_4$ is successfully synthesized.
- The hybrid coating layer is favorable for fast electron and Li^+ ion transport.
- The high rate and low temperature performances are enhanced via modifying with $CePO_4$.

ARTICLE INFO

Article history:
Received 3 May 2014
Received in revised form
28 June 2014
Accepted 30 June 2014
Available online 8 July 2014

Keywords:
Lithium iron phosphate
Cerous phosphate
Hybrid coating
High rate
Low temperature

ABSTRACT

Novel cerous phosphate and carbon hybrid coating $LiFePO_4$ cathode material successfully synthesized via liquid-phase precipitation reaction combined with the high temperature solid state method have been studied in lithium ion batteries. $LiFePO_4$ deposited an appropriate amount of cerous phosphate in carbon coating layer shows higher reversible capacity and stable cycle performance compared with the $LiFePO_4$/C. The good conductivity and stability of the hybrid coating layer can be favorable for these properties of $LiFePO_4$, which increase Li^+ ion and electronic transport on the surface and into the bulk of $LiFePO_4$ electrode, avoid HF dissolving $LiFePO_4$ in electrolyte, and facilitate the transfer kinetics. $LiFePO_4$/C–$CePO_4$ (1.0 mol%) electrode exhibits a stable cyclability and the highest capacity among all the $LiFePO_4$/C–$x CePO_4$ samples. The initial discharge capacity of $LiFePO_4$/C–$CePO_4$ (1.0 mol%) is 166.1, 161.4, 143.7 and 120.3 mAh g^{-1} at 1, 2, 5 and 10 C rates, respectively. And the capacity retention remains as high as 77.5% even after 650 cycles at 10 C. In addition, the material shows a higher reversible specific capacity of 100.9 mAh g^{-1} under lower discharging rate at −20 °C.

© 2014 Elsevier B.V. All rights reserved.

1. Introduction

Hybridization and electrification of vehicle propulsion systems have become main trends in the automotive industry in recent years. These trends are considered as primary instruments for increasing the total efficiency and decreasing or even eliminating carbon dioxide emissions or other pollutants from vehicles. Li^+ ion rechargeable batteries form key components not only for pure battery electric vehicles but also for intermediate storage of electrical energy in hybrid electric vehicles. As a well-known cathode material for lithium batteries, olivine structured $LiFePO_4$ has attracted extensive attention from both the academic and the industrial community. Indeed, this material has a high theoretical capacity of 170 mAh g^{-1} and can offer many inherent advantages such as safety, environmental benignity, and low toxicity [1–7]. However, the main drawbacks of this material are its intrinsic poor electrical conductivity (approximately 10^{-9}–10^{-10} S cm^{-1}) [8] and low Li^+ ion diffusivity coefficient (approximately 10^{-14}–10^{-16} cm^2 s^{-1}) [9], which are severely restricting the high rate and low temperature performance of $LiFePO_4$.

Numerous studies have been devoted to overcoming the intrinsic shortcomings of $LiFePO_4$. Up to now, one popular approach is surface coating of $LiFePO_4$ with carbon [10–15]. Since carbon coating was first utilized to improve the electronic conductivity of $LiFePO_4$, extensive research has been performed on its function of improving the physical as well as the electrochemical performance

* Corresponding author. State Key Laboratory of Metastable Materials Science and Technology, Yanshan University, Qinhuangdao 066004, China. Tel./fax: +86 335 8061569.
E-mail addresses: shaoguangjie@ysu.edu.cn (G. Shao), qinxj@ysu.edu.cn (X. Qin).

http://dx.doi.org/10.1016/j.jpowsour.2014.06.157
0378-7753/© 2014 Elsevier B.V. All rights reserved.

of $LiFePO_4$ [16–21]. The factors influencing the effect of the coating carbon include: carbon weight ratio and thickness, the conductivity of carbon, carbon uniformity, carbon-forming precursors, and so on. If the coating carbon has appropriate content, thin layer and complete graphitization on the surface of $LiFePO_4$, the electronic conductivity of $LiFePO_4$ will be greatly enhanced. Besides the direct contribution to electronic conductivity, the coating carbon may also bring some conductive metal phosphides during the synthesis process of $LiFePO_4$, which contributes to the increased electronic conductivity of $LiFePO_4$ [14,22]. While the charge and discharge process in $LiFePO_4$ electrode would involve a series of complex chemical and physical procedures at the interface of electrode/electrolyte [23–26]. And the most important step during the charging/discharging process is that the transferred electron must be reciprocally compensated by extraction/insertion of Li^+ ion to keep the charge balance. If the Li^+ ion diffusivity cannot attain the requisite diffusivity of the transferred electron, it will limit the transference of electron, leading to deteriorated electrochemical performance. Thus, an ideal coating layer for $LiFePO_4$ material should play multi-functional roles. For example, it should be highly conductive for both Li^+ ion and electrons, should facilitate easy solvation/desolvation of Li^+ ion, and provide reliable protection against HF attack, and so on. However, such a panacea can hardly be found in the existing coating materials. Instead, the combination of different coating materials, *e.g.*, to build a "hybrid coating layer", might be an alternative in the next stage, as shown in Fig. 1. Carbon shows excellent electronic conductivity among the reported coating materials, but it is not a good ionic conductor. Some good and stable Li^+ ion conductors coating on $LiFePO_4$ and other cathode materials (for instance: $LiMnO_2$, $LiCoO_2$, $LiNiO_2$) have demonstrated a great improvement in the electrochemical performance [27–32]. If carbon and Li^+ ion conductor materials can be co-coated on the surface of the $LiFePO_4$, the obtained hybrid coating layer would provide both high electronic and ionic conductivity for the core $LiFePO_4$ material. Such above mentioned hybrid coating might be a promising surface coating technique in the near future.

Cerous phosphate is of great interest for many applications, for example, it has been used as molecular sieves, catalysts supports, or optical materials [33–36]. Recently, the synthesis and electrochemical properties of $CePO_4$ have sparked considerable interest because they are believed to be potentially useful active coating materials and ionic conductor for lithium intercalation compounds in Li^+ ion batteries [37,38]. Compared with other Li^+ conductor (such as Al_2O_3, SnO_2, ZrO_2, TiO_2), the formation of a Li–Ce–P–O solid electrolyte coating layer for $CePO_4$ coated cathodes is more stable during the charge–discharge [37]. In this paper, in order to improve the high rate and low temperature performance of $LiFePO_4$, we successfully prepared $LiFePO_4$/C modified with $CePO_4$ via liquid-phase precipitation reaction combined with the high temperature solid state method. It is well known that rare earth element can remarkably improve the electrochemical performance of $LiFePO_4$/C by doping action [39–42]. However, from the research we found that the large size of cerium ion could not be doped into $LiFePO_4$, but yielded Li^+ ion conductor $CePO_4$ during the solid state reaction process. Compared with the single carbon coating $LiFePO_4$, we believe that Li^+ ion conductor $CePO_4$ and electronic conductor carbon hybrid coating layer can particularly enhance the high rate and low temperature performance of $LiFePO_4$.

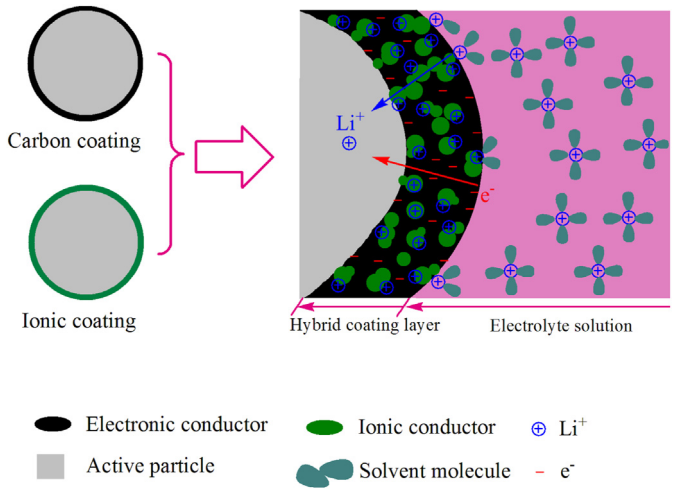

Fig. 1. Schematic illustration of the "electronic and ionic hybrid coating layer" for $LiFePO_4$ electrode material during charge/discharge processes.

2. Experimental

$LiFePO_4$/C–$x$$CePO_4$($x$ = 0, 0.5 mol%, 1.0 mol%, 2.0 mol%, 3.0 mol%, 4.0 mol%, 5.0 mol%) products were synthesized by liquid-phase precipitation reaction combined with the high temperature solid state method. 0.05 mol $NH_4H_2PO_4$ (AR) and 0.05 mol $FeSO_4 \cdot 7H_2O$ (AR) were first separately dissolved in 50 mL distilled water. The two aqueous solutions were pumped into a continuously stirred tank reactor. Proper H_2O_2 solution (30 wt%) was also pumped into the reactor to generate $FePO_4 \cdot xH_2O$ precipitation. To ensure proper reaction condition, temperature (25 °C) and stirring speed of the resulting mixture were precisely controlled throughout the synthesis process. The resulting $FePO_4$ hydrate powders were filtered, washed, and dried at 80 °C, then heat-treated at 500 °C for 3 h in air atmosphere to obtain crystalline anhydrous $FePO_4$ powders. $LiFePO_4$/C–$x$$CePO_4$ composites were synthesized by mixing the prepared $FePO_4$ powders with a stoichiometric amount of Li_2CO_3 (AR), a certain amount of CeO_2 (AR) and $NH_4H_2PO_4$ (AR), and superfluous citric acid. The mixture was then ball-milled for 6 h and finally calcined at 700 °C for 8 h under nitrogen atmosphere. The carbon content is 5% in the obtained powders. The method we adopted to measure the carbon content is dissolving the samples into hydrochloric acid solution. After filtrated and dried we get the residual carbon.

The crystal structure of the as-synthesized $LiFePO_4$/C–$x$$CePO_4$($x$ = 0, 0.5 mol%, 1.0 mol%, 2.0 mol%, 3.0 mol%, 4.0 mol%, 5.0 mol%) composites were analyzed using X-ray diffraction (XRD) on a Rigaku D/max-2500/pc. X-ray diffraction data were collected with the angle interval form 15°–55°(2θ). Field-emission scanning electron microscopy (FE-SEM) images and energy dispersive spectroscopy (EDS) maps of as-synthesized products were measured on a scanning electron microscopy (SEM, S-4800 operated at 10 kV). High-resolution transmission electron microscope (HR-TEM) images were measured on transmission electron microscopy (TEM) operated at 200 kV (Model JEM2010).

For lithium storage characterizations, the as-synthesized $LiFePO_4$/C–$x$$CePO_4$($x$ = 0, 0.5 mol%, 1.0 mol%, 2.0 mol%, 3.0 mol%, 4.0 mol%, 5.0 mol%) products were used as cathode materials for electrochemical test. The cathode electrode was fabricated by spreading the mixed slurry (80 wt% active material, 10 wt% polyvinylidene fluorid and 10 wt% acetylene black) onto an Al foil substrate, and then dried at 120 °C in a vacuum drying oven for 12 h. Half-cells were assembled by using $LiFePO_4$/C–$x$$CePO_4$ as working electrode, and lithium plate as counter and reference electrode. The electrolyte was 1 M $LiPF_6$ in a 1:1 V/V mixture of ethylene carbonate (EC) and dimethyl carbonate (DMC). The cell was tested in voltage windows between 2.4 V and 4.2 V (vs. Li) and operated on a Land battery testing system at ambient temperature (25 °C). In the galvanostatic intermittent titration technique (GITT)

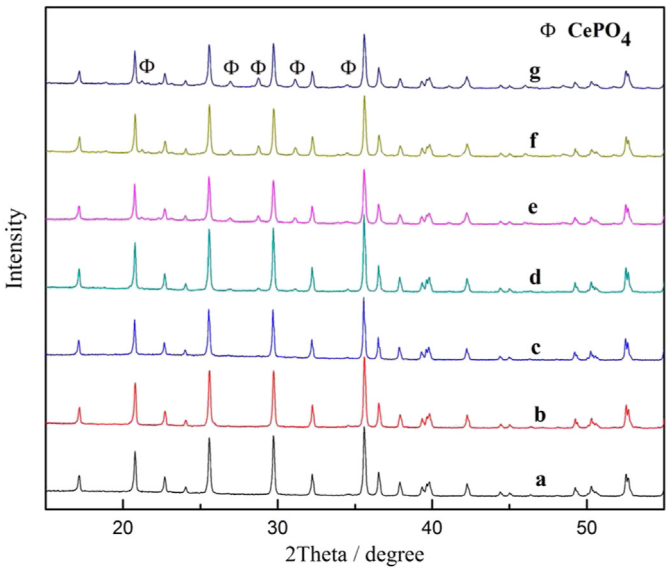

Fig. 2. Typical XRD patterns of $LiFePO_4/C–xCePO_4$ products with $x = 0$ (a), 0.5 mol% (b), 1.0 mol% (c), 2.0 mol% (d), 3.0 mol% (e), 4.0 mol% (f), 5.0 mol% (g).

experiment, the cell was charged at the rate of 0.05 C for 2 h followed by open circuit relaxation for 4 h. This step was repeated until a cut-off voltage of 4.2 V was reached and followed by a discharge process to reach a voltage of 2.4 V under the same setting condition. The electrochemical impedance spectra (EIS) tests (Frequency range from 0.01 to 100000 Hz) were performed on an electrochemical workstation CHI660E (Chenhua, Shanghai, China).

3. Results and discussion

3.1. Structure and morphology analysis

The phase purity and crystal structure of the products obtained were examined by X-ray diffraction (XRD). Illustrated in Fig. 2 are the typical XRD patterns of $LiFePO_4/C–xCePO_4$($x = 0$, 0.5 mol%, 1.0 mol%, 2.0 mol%, 3.0 mol%, 4.0 mol%, 5.0 mol%) products. All the patterns can be identified to be an orthorhombic olivine structure (JCPDS 83-2092) with a space group of *Pnma*. No obvious peaks corresponding to graphite are found in the XRD pattern, indicating that the carbon in the sample is not well crystallized [43]. It should be noted that the diffraction peaks of $CePO_4$ can be detected in all the cerous phosphate modified $LiFePO_4/C$ products.

The size and morphology of the products were examined by scanning electron microscopy (SEM). Fig. 3 shows SEM images of $LiFePO_4/C$ and $LiFePO_4/C–CePO_4$ ($x = 1.0$ mol%) products. It can be easily seen that the presence of $CePO_4$ has no significant influence on the morphology and size of the prepared products. Estimated by SEM, the sizes of the particles are mostly distributed from 100 to 300 nm. However, we can see that most of the $LiFePO_4/C$ particles congregate with each other in Fig. 3a and c. Interestingly, the dispersibility of $LiFePO_4/C–CePO_4$ ($x = 1.0$ mol%) particle becomes better (Fig. 3b and d) compared to that of $LiFePO_4/C$, which suggests that an appropriate amount of $CePO_4$ can effectively increase the interface between the particles and electrolyte, hence improve the ion and electronic conductivity of $LiFePO_4/C$. For further analysis of $LiFePO_4/C–CePO_4$ ($x = 1.0$ mol%), energy-dispersive X-ray spectrometry (EDS) mappings were carried out, as illustrated in Fig. 4. Fig. 4a shows a typical SEM image of $LiFePO_4/C–CePO_4$ nanoparticle, and Fig. 4b–f give recorded maps of Ce, C, O, P and Fe signals. From the result we can see that the Ce–K and C–K signals are detected all through the particle, indicating that $CePO_4$ and carbon were homogeneously distributed on the entire $LiFePO_4$ surface.

The microstructure and surface morphology of the as-synthesized material were further characterized by transmission electron microscopy (TEM) and high resolution TEM (HR-TEM). Fig. 5 illustrates the TEM images of samples $LiFePO_4/C$ and $LiFePO_4/C–CePO_4$. From images a and b in Fig. 5, it is seen that both the particles of $LiFePO_4/C$ and $LiFePO_4/C–CePO_4$ are composed of sphere-like nanoparticles. The TEM images (Fig. 5a and b) from the edge of these nanoparticles reveal that they have a relatively smooth and closed structure, covered with a coating layer. The related SAED patterns (the inset in Fig. 5a and b) exhibit a regular

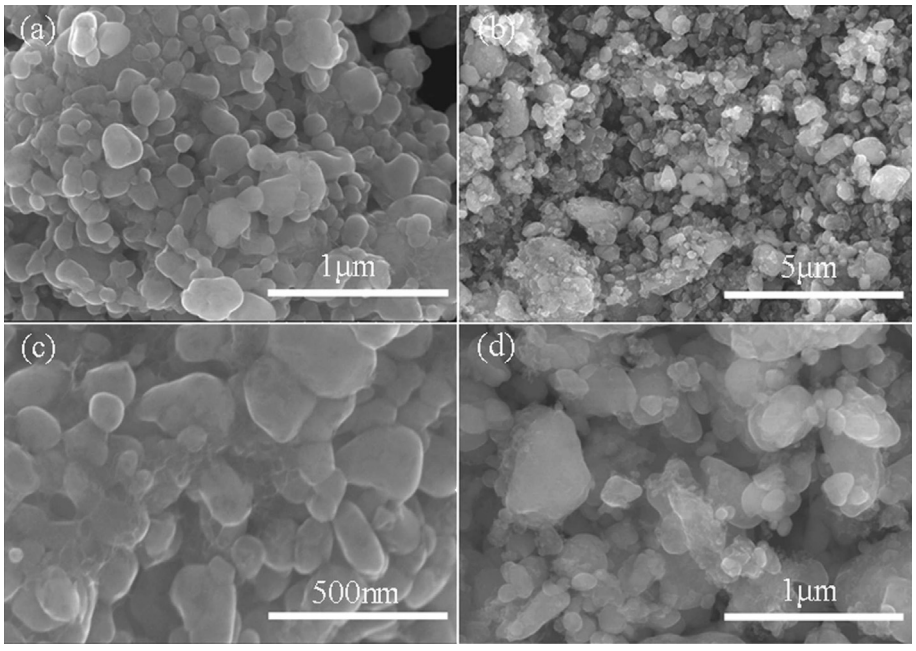

Fig. 3. SEM images of $LiFePO_4/C$ (a, c) and $LiFePO_4/C–CePO_4$ ($x = 1.0$ mol%) products (b, d).

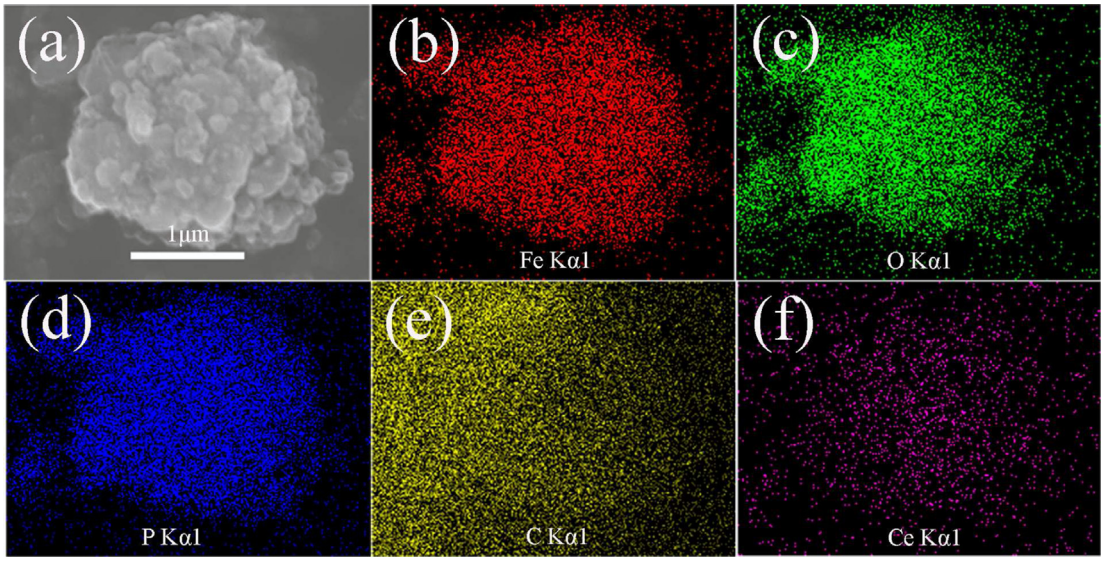

Fig. 4. Energy-dispersive X-ray spectrometry (EDS) mappings of $LiFePO_4$/C– $CePO_4$ (x = 1.0 mol%) products.

and clear diffraction spot array, which indicate that the particle is single-crystalline and can be indexed as the $LiFePO_4$ orthorhombic phase. In addition, high resolution TEM (HR-TEM) images of $LiFePO_4$/C and $LiFePO_4$/C–$CePO_4$ are given in Fig. 5c and d. It is clearly seen from the HR-TEM images in Fig. 5c and d that the surface of the two $LiFePO_4$ samples is covered by amorphous coating layer with the same thickness (*ca.* 3–4 nm). However, the difference of the coating layer is that the hybrid coating layer is

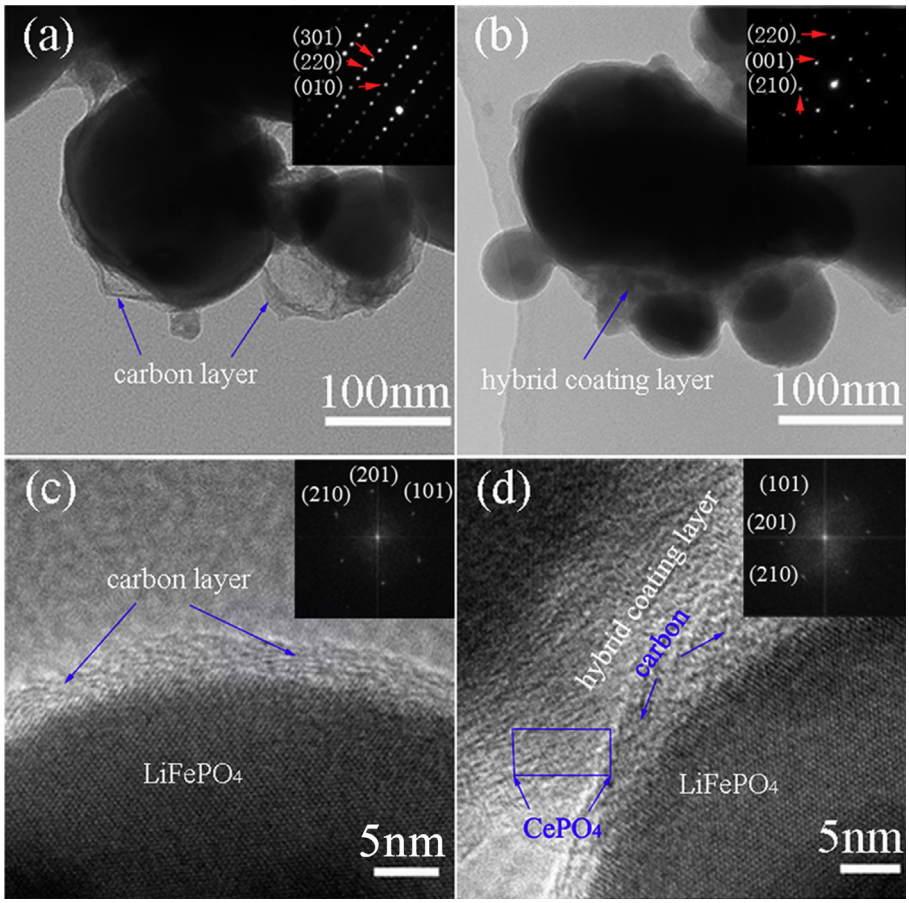

Fig. 5. TEM images of samples $LiFePO_4$/C (a) and $LiFePO_4$/C–$CePO_4$ (1.0 mol%) (b). The inset image is the corresponding SAED (selected area electron diffraction). HR-TEM images of samples $LiFePO_4$/C (c) and $LiFePO_4$/C–$CePO_4$ (1.0 mol%) (d). The inset image is the corresponding Fast Fourier Transform pattern.

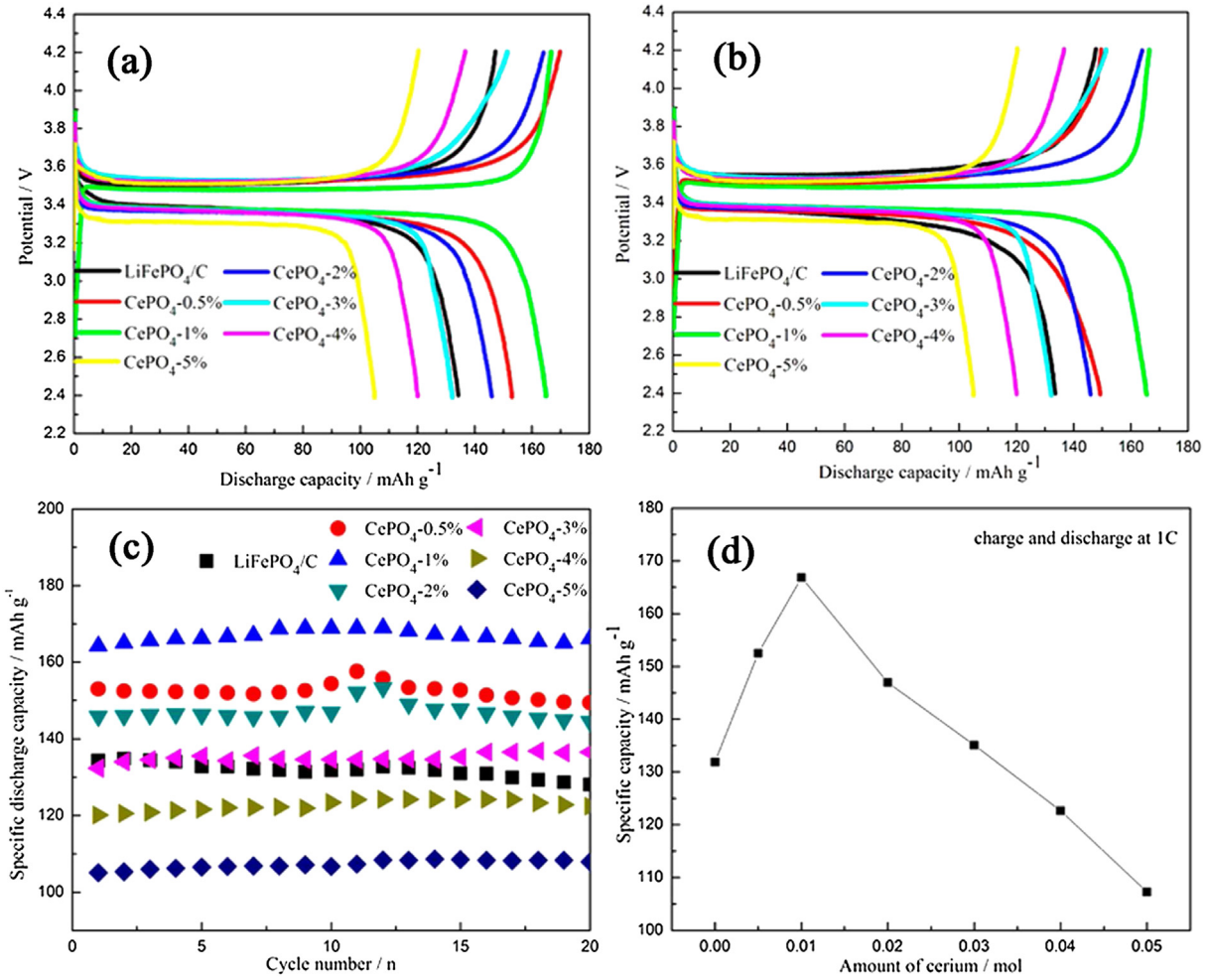

Fig. 6. Typical galvanostatic curves of all electrodes in the 1st (a) and 20th (b) discharge/charge cycle at rate of 1 C, discharge/charge curves of all electrodes in the 20th cycle (c), and the average discharge capacity of all electrodes in 20 cycles at 1 C rate (d).

fabricated in the surface of $LiFePO_4$/C–$CePO_4$ sample due to the presence of $CePO_4$ nanoparticles with the size of 5 nm (as shown in Fig. 5d). Compared with the carbon coating layer (Fig. 5c), the hybrid coating is thought to be favorable for fast Li^+ ion and electronic transport and preventing direct contact between electrolyte and $LiFePO_4$. The inset in Fig. 5c and d is corresponding to fast Fourier transform (FFT) pattern, which also indicates the single crystal characteristics of the nanoparticles. These results are in good agreement with the results of XRD, further confirming that the presence of $CePO_4$ has no significant influence on the morphology and microstructure of $LiFePO_4$/C.

To test the electrochemical lithium storage behavior of the prepared products, simulative cells using a $LiFePO_4$/C–$x CePO_4$(x = 0, 0.5 mol%, 1.0 mol%, 2.0 mol%, 3.0 mol%, 4.0 mol%, 5.0 mol%) cathode and lithium anode are charged and discharged between 2.4 and 4.2 V Fig. 6a and b shows cell voltage *vs* specific capacity for all electrodes at the 1st and 20th discharge/charge cycles at the rate of 1 C. It can be found that all the cells exhibit one charge or discharge plateau around 3.45 V, which reflects that the process of lithium deposition and dissolution is smooth in every case. As for the discharge initial capacity, interestingly, the electrode containing $LiFePO_4$/C–$CePO_4$ (1.0 mol%) exhibits a discharge capacity of 164.2 mAh g^{-1} at a current rate of 1 C, which is much higher than those of $LiFePO_4$/C–$x CePO_4$ (133.6, 153, 145.9, 132.3, 120.1 and 105.1 mAh g^{-1} for x = 0, 0.5 mol%, 2.0 mol%, 3.0 mol%, 4.0 mol% and 5.0 mol%, respectively). Moreover, we can see form Fig. 6b that after 20 cycles $LiFePO_4$/C–$CePO_4$ (1.0 mol%) electrode still retains a reversible capacity of 166.1 mAh g^{-1}. Additionally, Fig. 6c and d displays specific capacity versus discharge cycle curves and the average discharge capacity of all the electrodes in 20 cycles at 1 C rate, respectively. It is seen that $LiFePO_4$/C–$CePO_4$ (1.0 mol%) electrode performs a stable cyclability and the highest capacity among all samples.

For further test, Fig. 7 shows the performances of $LiFePO_4$/C and $LiFePO_4$/C–$CePO_4$ (1.0 mol%) electrodes at various discharge rates. Fig. 7a and b illustrate typical voltage–capacity curves of $LiFePO_4$/C and $LiFePO_4$/C–$CePO_4$ (1.0 mol%) electrodes at the rate of 1, 2, 5, and 10 C, respectively. It is recorded that $LiFePO_4$/C–$CePO_4$ (1.0 mol%) electrode gives discharge capacities of 166.1, 161.4, 143.7 and 120.3 mAh g^{-1} at 1, 2, 5 and 10 C rates, which is much higher than that of $LiFePO_4$/C electrode which achieves capacities of 133.6, 119, 74.4, and 41.5 mAh g^{-1}, respectively. Besides, from images c and d in Fig. 7, we can see that $LiFePO_4$/C–$CePO_4$ (1.0 mol%) electrode exhibits excellent performance for Li^+ storage with higher capacity and rate capability than that of $LiFePO_4$/C. The $LiFePO_4$/C–$CePO_4$ (1.0 mol%) sample also demonstrates superior electrochemical performance under a long term cyclic test at 10 C rate, as shown in Fig. 8. The coulombic efficiency remains constant at 96%. The cell retains about 77.5% of its initial capacity after 650 cycles at the rate as high as 10 C. The superior cycling performance can be attributed

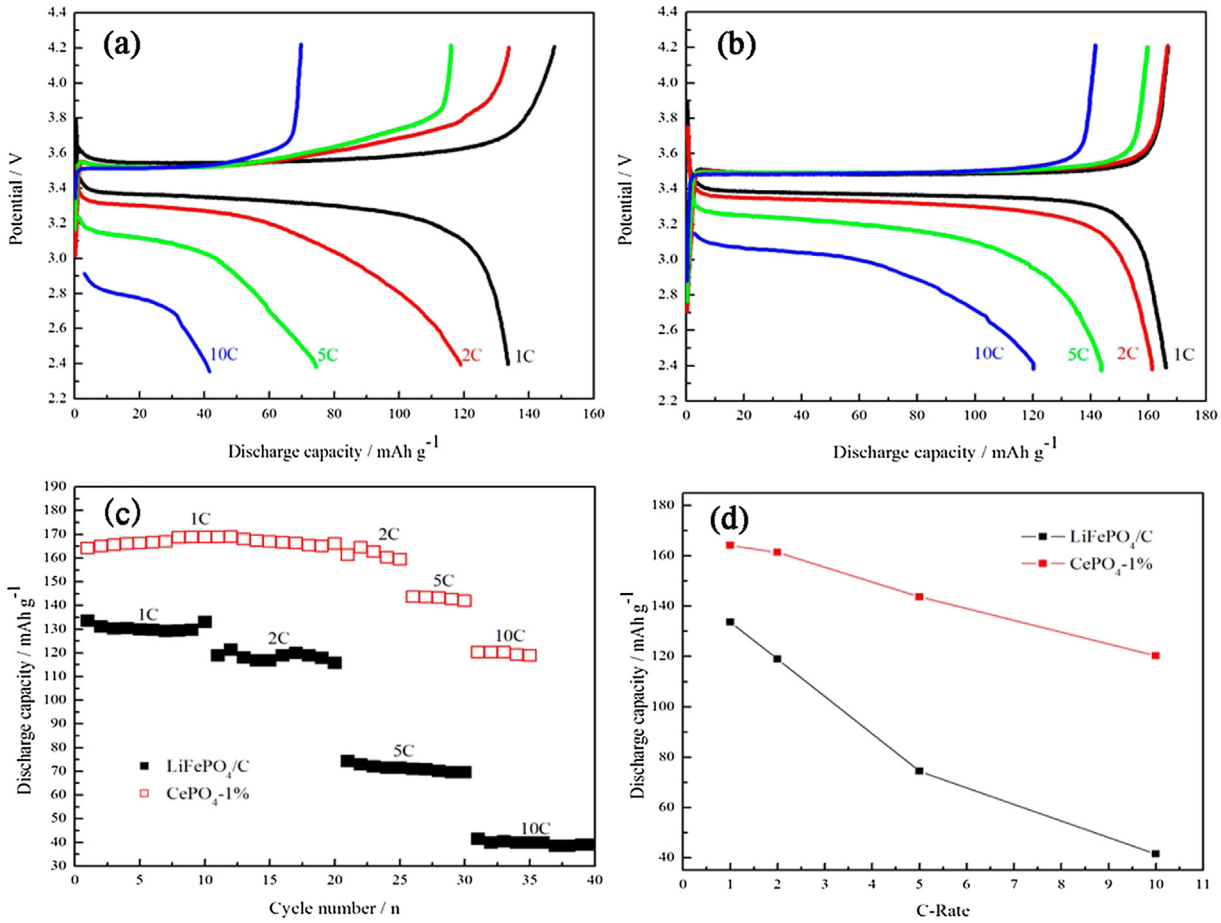

Fig. 7. Typical voltage–capacity curves of $LiFePO_4$/C (a) and $LiFePO_4$/C–$CePO_4$ (1.0 mol%) (b) electrodes at rate of 1, 2, 5, and 10 C, respectively. The cycling performance (c) and rate capacity retention (d) of $LiFePO_4$/C and $LiFePO_4$/C–$CePO_4$ (1.0 mol%) electrodes at various rates.

to the structural stability of $LiFePO_4$, the better hybrid coating layer and the enhancement of ionic and electronic conductivity in the electrode.

The electrochemical measurement has also been carried out at lower temperature. Fig. 9 shows the initial charge–discharge curves of the $LiFePO_4$/C sample and $LiFePO_4$/C–$CePO_4$ (1.0 mol%) sample under various rates at −20 °C. The $LiFePO_4$/C–$CePO_4$ (1.0 mol%) electrode shows discharge capacity of 100.9, 74.7 and 35.5 mAh g^{-1} at 0.2 C, 0.5 C and 1 C rates, respectively. It is concluded that the low temperature performance of $LiFePO_4$/C–$CePO_4$ (1.0 mol%) sample is better than that of the $LiFePO_4$/C sample. At lower temperature the electrochemical catalytic activity of electrodes declines and the polarization influence becomes more dominant. However, the unfavorable factors can be improved by hybrid coating with ionic conductor $CePO_4$ and carbon. That is also confirmed by impedance spectroscopy.

GITT technique has been used to investigate the kinetic performance of the electrode materials. Even though it is designed for studying the chemical diffusion coefficient in solid solution systems, it can provide comparative information of the electrode kinetic through the voltage relaxation time to equilibrium potential and the magnitude of overpotential. To study the influence of $CePO_4$ on the kinetic reaction of $LiFePO_4$ electrode, GITT curves of the $LiFePO_4$/C and $LiFePO_4$/C–$CePO_4$ (1.0 mol%) are performed as shown in Fig. 10. It can be seen from Fig. 10a that the $LiFePO_4$/C–$CePO_4$ (1.0 mol%) sample shows a narrower equilibrium potential hysteresis and lower polarization than the $LiFePO_4$/C sample. The magnified dotted region in Fig. 10a was shown in Fig. 10b. The $LiFePO_4$/C–$CePO_4$ (1.0 mol%) electrode has smaller polarization overpotential than the $LiFePO_4$/C sample, which indicates the much faster kinetics of $LiFePO_4$/C–$CePO_4$ (1.0 mol%) than that of the sample $LiFePO_4$/C as exemplified by the much shorter relaxation

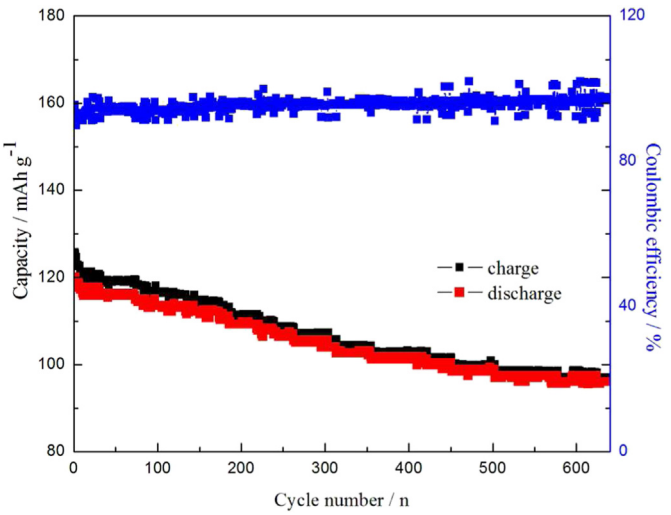

Fig. 8. Life test of $LiFePO_4$/C–$CePO_4$ (1.0 mol%) electrode at 10 C rate.

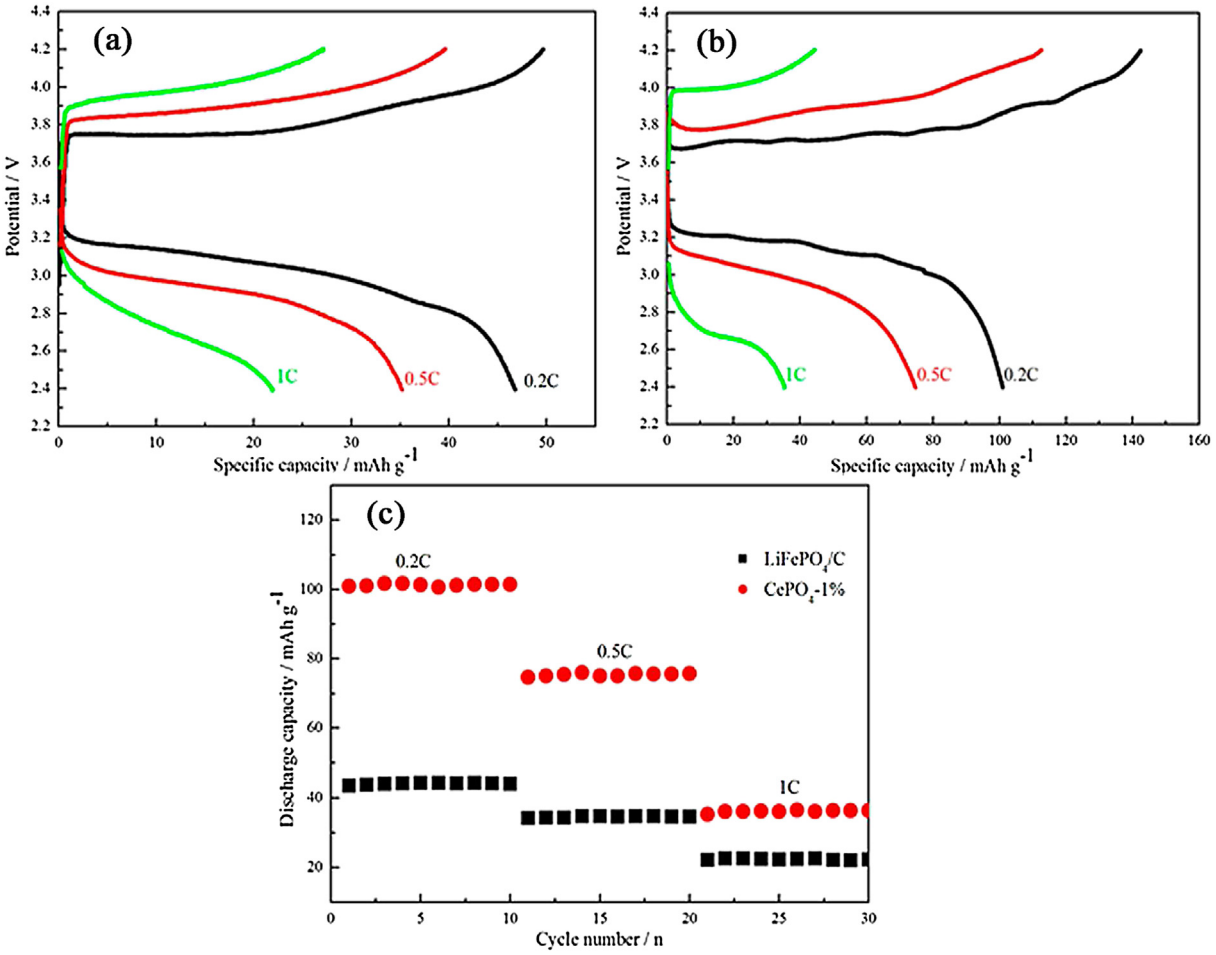

Fig. 9. The initial charge–discharge curves of the $LiFePO_4$/C sample (a) and $LiFePO_4$/C–$CePO_4$ (1.0 mol%) sample (b) under various rates at −20 °C. The cycling performance of $LiFePO_4$/C and $LiFePO_4$/C–$CePO_4$ (1.0 mol%) electrodes under various rates at −20 °C (c).

time it takes to reach the equilibrium potential. This is the reason why the hybrid coating layer of $CePO_4$ and carbon can notably improve the electrochemical performance of the material.

The electrochemical impedance spectra (EIS) is used to further analyze the effect of $CePO_4$ on the electrode reaction impedance and ion diffusion. The electrodes were conducted at 50% of discharge or charge state to avoid the huge potential change brought by small current alternation during EIS measurements. Fig. 11a and b shows EIS of the $LiFePO_4$/C and $LiFePO_4$/C–$CePO_4$ (1.0 mol%) electrodes at various temperatures. An EIS spectrum is composed of a semicircle at high frequency range and an inclined line within the low frequency range. The resistance of the

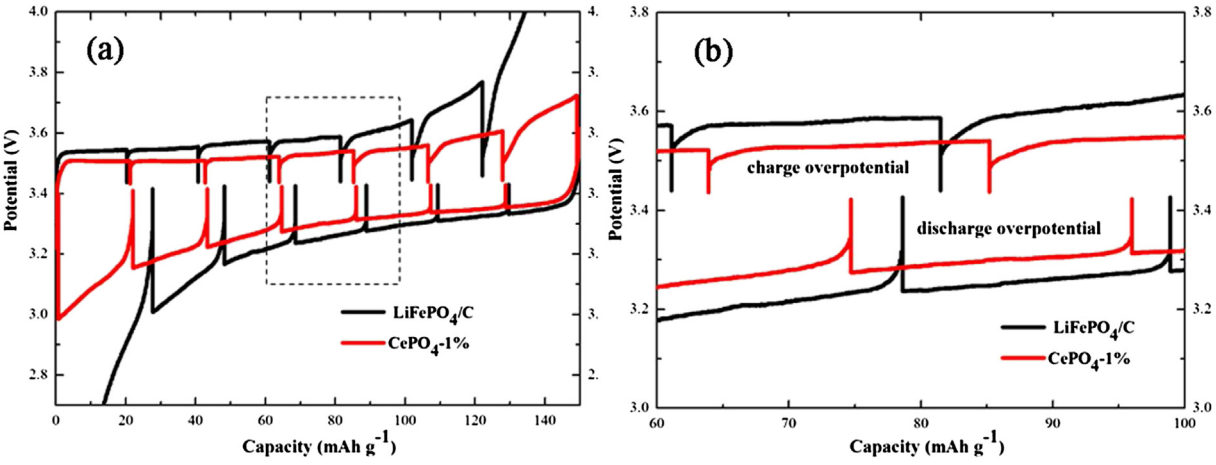

Fig. 10. GITT curves of the $LiFePO_4$/C and $LiFePO_4$/C–$CePO_4$ (1.0 mol%) electrodes (a) and the magnified dotted region (b).

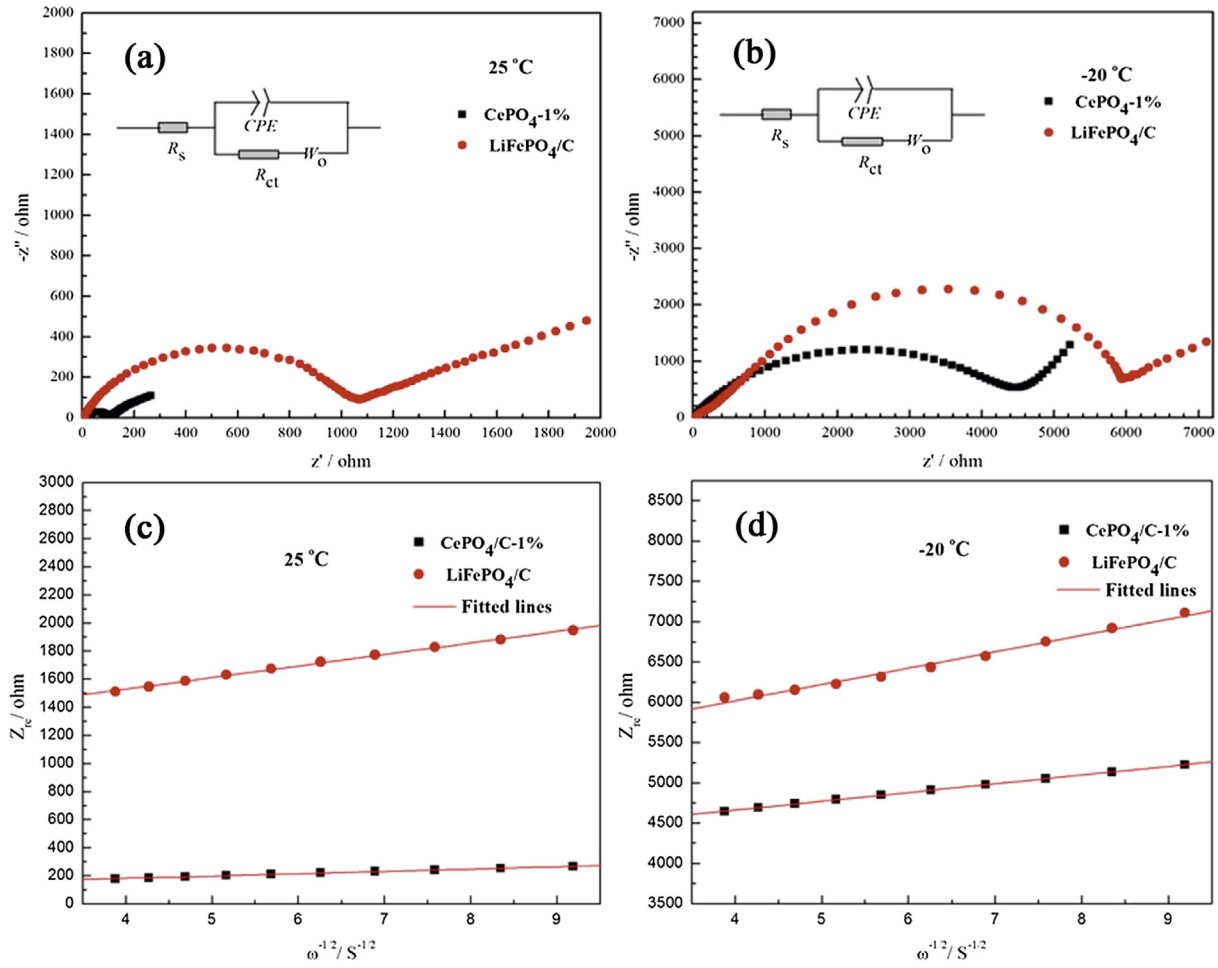

Fig. 11. EIS for $LiFePO_4$/C and $LiFePO_4$/C–$CePO_4$ (1.0 mol%) electrodes at 25 °C (298 K) (a) and −20 °C (253 K) (b). The plot of Z_{re} *vs*. the reciprocal root square of the lower angular frequencies ($\omega^{-1/2}$) for $LiFePO_4$/C and $LiFePO_4$/C–$CePO_4$ (1.0 mol%) electrodes at 25 °C (298 K) (c) and −20 °C (253 K) (d). The inset image is the corresponding equivalent circuit.

semicircle is attributed to the charge transfer process. It can be seen clearly from Fig. 11a and b that the charge transfer resistance (R_{ct}) of $LiFePO_4$/C–$CePO_4$ (1.0 mol%) electrode is lower than that of the $LiFePO_4$/C electrode at 25 °C (298 K) and −20 °C (253 K), indicating the hybrid coating layer significantly suppresses the rise of the transfer resistance of $LiFePO_4$ material at both room and low temperature. The Nyquist plots are fitted using the equivalent circuit (the inset of Fig. 11a and b) and the derived impedance parameters are listed in Table 1. However, the inclined line in EIS spectrum is attributed to the diffusion of the lithium ions into the bulk of the electrode material, the so-called Warburg diffusion. The Warburg coefficient σ can be obtained by equation [44] (1):

$$Z_{re} = R_e + R_{ct} + \sigma\omega^{-1/2} \quad (1)$$

where R_e is the resistance of the electrolyte, R_{ct} is the charge transfer resistance and ω is the angular frequency in the low frequency region and Z_{re} is the real axis resistance in the low frequency region. Both R_e and R_{ct} are kinetics parameters independent of frequency. Then σ is the slope for the plot of Z_{re} *vs*. the reciprocal root square of the lower angular frequencies ($\omega^{-1/2}$). The plot of Z_{re} *vs*. the reciprocal root square of the lower angular frequencies ($\omega^{-1/2}$) for the $LiFePO_4$/C and $LiFePO_4$/C–$CePO_4$ (1.0 mol%) electrodes at different temperature are shown in Fig. 11c and d. The slope of the fitted line is the Warburg coefficient σ. In addition, the Li^+ ion diffusion rates are determined by the following equation [45] (2):

$$D = R^2T^2 \Big/ 2A^2n^4F^4C^2\sigma^2 \quad (2)$$

where R is the gas constant, T is the absolute temperature (K), F is the Faraday constant, A is the surface area of the $LiFePO_4$ cathode, n is the number of electrons during the process of Li^+ ion transportation, C is the molar concentration of Li^+ ion in the $LiFePO_4$ cathode and σ is the Warburg coefficient. The Li^+ ion diffusion coefficient of the two electrodes at 25 °C (298 K) and −20 °C (253 K) are also listed in Table 1. At 25 °C (298 K), the lithium diffusion coefficient of the $LiFePO_4$/C and $LiFePO_4$/C–$CePO_4$ (1.0 mol%) is 1.64×10^{-14} cm^2 S^{-1} and 4.03×10^{-13} cm^2 S^{-1}, respectively. The higher D obtained after $CePO_4$ modification is attributed to higher ionic conductivity, and leads to the enhancement of the high rate performance at room temperature. These results are in good agreement with the charge/discharge characteristics. As the

Table 1
Result of the electrochemical impedance for $LiFePO_4$/C and $LiFePO_4$/C–$CePO_4$ electrodes at 25 °C (298 K) (a) and −20 °C (253 K).

sample	R_{ct} (Ω)		D (cm^2 S^{-1})		I_0 (mA g^{-1})	
	25 °C	−20 °C	25 °C	−20 °C	25 °C	−20 °C
$LiFePO_4$/C	953.7	5639	1.64×10^{-14}	1.94×10^{-15}	27	4
$LiFePO_4$/C–$CePO_4$	96.5	4439.34	4.03×10^{-13}	6.84×10^{-15}	266	5

temperature decreases to −20 °C (253 K), the lithium diffusion coefficient of the $LiFePO_4$/C and $LiFePO_4$/C–$CePO_4$ (1.0 mol%) decreases to 1.94×10^{-15} cm^2 S^{-1} and 6.84×10^{-15} cm^2 S^{-1}, respectively which illustrate that the decrease in chemical diffusion coefficient is the most important factor that limits the low temperature performance of $LiFePO_4$ materials. Nevertheless, even at low temperature, the lithium diffusion coefficient of $LiFePO_4$/C–$CePO_4$ (1.0 mol%) is higher than that of the $LiFePO_4$. The above analysis indicates that the enhancement of low temperature performance for $LiFePO_4$/C–$CePO_4$ (1.0 mol%) materials is attributed the improvement of the lithium ion diffusivity in the bulk $LiFePO_4$.

In addition, exchange current density (I_0) is a very important parameter of kinetics for an electrochemical reaction, which can be used to measure the electrochemical activity of electrodes. It is calculated by the following formula (3) and the results are listed in Table 1.

$$I_0 = RT/nR_{ct}F \quad (3)$$

where R is the gas constant, T is the absolute temperature, n is the charge transfer number, R_{ct} is the charge transfer resistance and F is the Faraday constant. It is apparently seen in Table 1 that the value of exchange current density (I_0) for $LiFePO_4$/C–$CePO_4$ (1.0 mol%) electrode is obviously higher than that of $LiFePO_4$/C at 25 °C (298 K) and −20 °C (253 K). The larger value of exchange current density (I_0) indicates that the transfer of lithium–ion and electron are more feasible on the electrode modified with ionic conductor $CePO_4$ and carbon hybrid coating layer, which is beneficial to overcoming the restriction of kinetics in the charge/discharge process and improve the high rate and low temperature performance of the material.

4. Conclusions

Olivine structured $LiFePO_4$/C–$xCePO_4$($x = 0$, 0.5 mol%, 1.0 mol%, 2.0 mol%, 3.0 mol%, 4.0 mol%, 5.0 mol%) ($x = 0$, 0.01, 0.02, 0.03, 0.04, 0.05) composites have been synthesized by liquid-phase precipitation reaction method combined with the high temperature solid state method. The carbon and $CePO_4$ hybrid coating layer was thin, homogeneous and was stacked well on the surface of $LiFePO_4$. An appropriate content of $CePO_4$ and carbon hybrid coating, as a good ionic and electronic conductor, which enhanced the ionic and electronic transport in the $LiFePO_4$ electrode so as to facilitate the mass and charge transfer and improving the reversible capacity of $LiFePO_4$ electrode. It also protected the $LiFePO_4$ electrode from electrolyte corrosion and maintained the structural stability of the $LiFePO_4$, thus resulting in much improved rate and low temperature capability and cycle stability of the $LiFePO_4$.

Acknowledgments

We are grateful for the financial support from the Natural Science Research Keystone Program of Universities in Hebei Province China (No. ZH2011228) and the Natural Science Foundation in Hebei Province China (No. B2012203069).

References

[1] M. Yonemura, A. Yamada, Y. Takei, N. Sonoyama, R. Kanno, J. Electrochem. Soc. 151 (2004) A1352.
[2] A.K. Padhi, K.S. Nanjundaswamy, J.B. Goodenough, J. Electrochem. Soc. 144 (1997) 1188.
[3] G.W. Wang, S. Bewlay, J. Yao, J.H. Ahn, S.X. Dou, H.K. Liu, Electrochem. Solid State Lett. 7 (2004) A503.
[4] H. Huang, S.C. Yin, L.F. Nazar, Electrochem. Solid State Lett. 4 (2001) A170.
[5] F. Sauvage, E. Baudrin, L. Gengembre, J.M. Tarascon, Solid State Ionics 176 (2005) 1869.
[6] D.D. MacNeil, Z. Lu, Z. Chen, J.R. Dahn, J. Power Sources 108 (2002) 8.
[7] M. Takahashi, S.I. Tobishima, K. Takei, Y. Sakurai, Solid State Ionics 148 (2002) 283.
[8] S.Y. Chung, J.T. Bloking, Y.M. Chiang, Nat. Mater. 1 (2002) 123.
[9] P.P. Prosini, M. Lisi, D. Zane, M. Pasquali, Solid State Ionics 148 (2002) 45.
[10] G. Huang, W. Li, H. Sun, J. Wang, J. Zhang, H. Jiang, F. Zhai, Electrochim. Acta 97 (2013) 92.
[11] Z. Chen, B. Du, M. Xu, H. Zhu, L. Li, W. Wang, Electrochim. Acta 109 (2013) 262.
[12] G. Qin, Q. Ma, C. Wang, Electrochim. Acta 115 (2014) 407.
[13] Y. Zhou, J. Wang, Y. Hu, R. OHayre, Z. Shao, Chem. Commun. 46 (2010) 7151.
[14] B. Zhao, X. Yu, R. Cai, R. Ran, H. Wang, Z. Shao, J. Mater. Chem. 22 (2012) 2900.
[15] X. Zhang, X. Zhang, W. He, Y. Yue, H. Liu, J. Ma, Chem. Commun. 48 (2012) 10093.
[16] J. Wang, J. Yang, Y. Tang, R. Li, G. Liang, T.K. Sham, X. Sun, J. Mater. Chem. 1 (2013) 1579.
[17] J. Yang, J. Wang, Y. Tang, D. Wang, X. Li, Y. Hu, R. Li, G. Liang, T.K. Sham, X. Sun, Energy Environ. Sci. 6 (2013) 1521.
[18] H. Ji, L. Zhang, M.T. Pettes, H. Li, S. Chen, L. Shi, R. Piner, R.S. Ruoff, Nano Lett. 12 (2012) 2446.
[19] G. Qin, Q. Wu, J. Zhao, Q. Ma, C. Wang, J. Power Sources 248 (2014) 588.
[20] C. Gong, Z. Xue, X. Wang, X.P. Zhou, X.L. Xie, Y.W. Mai, J. Power Sources 246 (2014) 260.
[21] J. Li, Q. Qu, L. Zhang, H. Zheng, J. Alloys Compd. 579 (2013) 377.
[22] B. Kang, G. Ceder, Nature 458 (2009) 190.
[23] L.X. Yuan, Z.H. Wang, W.X. Zhang, X.L. Hu, J.T. Chen, Y.H. Huang, Energy Environ. Sci. 4 (2011) 269.
[24] M.S. Islam, D.J. Driscoll, C.A.J. Fisher, P.R. Slater, Chem. Mater. 20 (2005) 5085.
[25] D. Morgan, A. Van der Ven, G. Ceder, Electrochem. Solid State Lett. 7 (2004) A30.
[26] S. Nishimura, G. Kobayashi, K. Ohoyama, R. Kanno, M. Yashima, A. Yamada, Nat. Mater. 9 (2008) 707.
[27] G. Tan, F. Wu, L. Li, R. Chen, S. Chen, J. Phys. Chem. C. 117 (2013) 6013.
[28] J. Yao, F. Wu, X. Qiu, N. Li, Y. Su, Electrochim. Acta 56 (2011) 5587.
[29] S.X. Zhao, H. Ding, Y.C. Wang, B.H. Li, C.W. Nan, J. Alloys Compd. 566 (2013) 206.
[30] Q. Zhang, W. Jiang, Z. Zhou, S. Wang, X. Guo, S. Zhao, G. Ma, Solid State Ionics 218 (2012) 31.
[31] J. Lu, Q. Peng, W. Wang, C. Nan, L. Li, Y. Li, J. Am. Chem. Soc. 135 (2013) 1649.
[32] Y.C. Lu, A.N. Mansour, N. Yabuuchi, Y. Shao-Horn, Chem. Mater. 21 (2009) 4408.
[33] D. Kashiwagi, A. Takai, T. Takubo, H. Yamada, T. Inoue, K. Nagaoka, Y. Takita, J. Colloid Interface Sci. 332 (2009) 136.
[34] G. Li, K. Chao, H. Peng, K. Chen, Z. Zhang, J. Phys. Chem. C. 112 (2008) 16452.
[35] J. Han, L. Wang, S.S. Wong, J. Phys. Chem. C. 118 (2014) 5671.
[36] G. Chen, H. Zhao, F. Rosei, D. Ma, J. Phys. Chem. C. 117 (2013) 10031.
[37] J. Kim, M. Noh, J. Cho, H. Kim, K.B. Kim, J. Electrochem. Soc. 152 (2005) A1142.
[38] W. Quan, Z. Tang, J. Zhang, Z. Zhang, Mater. Chem. Phys. 147 (2014) 333.
[39] H. Zhang, Y. Xu, C. Zhao, X. Yang, Q. Jiang, Electrochim. Acta 83 (2012) 341.
[40] Q. Zhang, S. Wang, Z. Zhou, G. Ma, W. Jiang, X. Guo, S. Zhao, Solid State Ionics 191 (2011) 40.
[41] D. Tong, F. Luo, W. Chu, Y. Li, P. Wu, 124 (2010) 1.
[42] X. Zhao, X. Tang, L. Zhang, M. Zhao, J. Zhai, Electrochim. Acta 55 (2010) 5899.
[43] Y.Q. Wang, J.L. Wang, J. Yang, Y.N. Niu, Adv. Funct. Mater. 16 (2006) 2135.
[44] C. Yan, X. Zhao, R. Guo, Electrochim. Acta 55 (2010) 922.
[45] L. Wang, P. Ma, K. Zhang, C. Gao, C. Yan, J. Salt Lake Res. 17 (2009) 52.